analytical chemistry

Article

Cite This: *Anal. Chem.* 2018, 90, 4733−4740

pubs.acs.org/ac

Point-of-Care Determination of Acetaminophen Levels with Multi-Hydrogen Bond Manipulated Single-Molecule Recognition (eMuHSiR)

Yan Zhang,[†,‡] Zhongyuan Huang,[†,§] Letao Wang,[‡] Chunming Wang,[‡] Changde Zhang,[†] Tomas Wiese,[∥] Guangdi Wang,[†] Kevin Riley,[†] and Zhe Wang[†,*]

[†]Department of Chemistry, Xavier University of Louisiana, New Orleans 70125, United States

[‡]College of Chemistry and Chemical Engineering, Lanzhou University, Lanzhou 730000, China

[§]College of Chemistry and Chemical Engineering, Xinyang Normal University, Xinyang 464000, China

[∥]College of Pharmacy, Xavier University of Louisiana, New Orleans 70125, United States

Supporting Information

ABSTRACT: This work aims to face the challenge of monitoring small molecule drugs accurately and rapidly for point-of-care (POC) diagnosis in current clinical settings. Overdose of acetaminophen (AP), a commonly used over the counter (OTC) analgesic drug, has been determined to be a major cause of acute liver failure in the US and the UK. However, there is no rapid and accurate detection method available for this drug in the emergency room. The present study examined an AP sensing strategy that relies on a previously unexplored strong interaction between AP and the arginine (Arg) molecule. It was found that as many as 4 hydrogen bonds can be formed between one Arg molecule and one AP molecule. By taking advantages of this structural selectivity and high tenability of hydrogen bonds, Arg, immobilized on a graphene surface via electrostatic interactions, was utilized to structurally capture AP. Interestingly, bonded AP still remained the perfect electrochemical activities. The extent of Arg−AP bonds was quantified using a newly designed electrochemical (EC) sensor. To verify the feasibility of this novel assay, based on multihydrogen bond manipulated single-molecule recognition (eMuHSiR), both pharmaceutical and serum sample were examined. In commercial tablet measurement, no significant difference was seen between the results of eMuHSiR and other standard methods. For measuring AP concentration in the mice blood, the substances in serum, such as sugars and fats, would not bring any interference to the eMuHSiR in a wide concentration range. This eMuHSiR method opens the way for future development of small molecule detection for the POC testing.

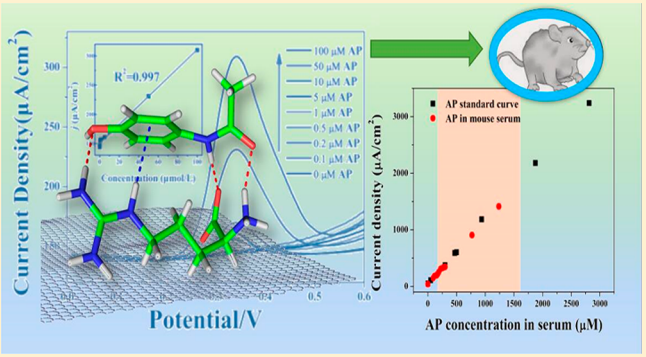

Acetaminophen (N-acetyl-*p*-aminophenol or paracetamol, AP), a commonly used over-the-counter (OTC) analgesic and fever reducer, may cause serious acute liver injury and irreversible hepatic failure that can result in death or need for emergency liver transplantation when consumed in overdose quantities.[1] Currently, AP toxicity has replaced viral hepatitis as the most common cause of acute liver failure (39% of cases) in the United States. There are about 78 000 people sent to the emergency room, 33 000 hospitalizations, and 150 deaths because of AP overdose every year.[2−4] AP hepatotoxicity does not result from AP itself but its metabolites. AP is converted by the drug metabolizing enzymes to reactive metabolites, mainly *N*-acetyl-*p*-benzoquinone imine (NAPQI), which can occur in a complex mechanistic sequence by rapidly depleting the glutathione and covalently bonding to nucleophilic aspects of the cell. As a result, hepatic necrosis begins to develop and can progress to acute liver failure within 48 h. The efficacy of treatment is greatly enhanced within the first 8 h, with a stepwise increase in hepatotoxicity with increasing treatment delays between 8 and 16 h. The detailed interpretation is required to ensure that peak levels have been achieved in Rumack−Matthew nomogram[5] with the conventional procedure.[6,7] This method, therefore, is not predictive of impending hepatic necrosis, and diagnosis typically is not possible until three to 5 days after ingestion. However, an overdose may occur intentionally or accidentally from over-the-counter AP and the initial clinical symptoms of AP toxicity are relatively mild and nonspecific. For these reasons, monitoring AP concentration in serum becomes paramount not only for the proper assessment of the severity of overdose but also for

Received: December 21, 2017
Accepted: March 15, 2018
Published: March 15, 2018

DOI: 10.1021/acs.analchem.7b05361
Anal. Chem. 2018, 90, 4733−4740

appropriate therapeutic decision making,[8,9] even in the absence of symptoms.

Typically, indirect methods targeting the nontoxic metabolites of AP may cause misleading results. To accurately measure the concentration of such a small molecule in serum, a special separation processes must be performed and combined with other detection methods, such as liquid chromatography,[10] titrimetry,[11] capillary electrophoresis,[12] or chemiluminescence.[13] For rapid clinical tests, immunoassay has been considered as a relatively specific method for AP detection, with spectrophotometric methods used to measure the hydrolyzed AP. These methods, in which the absorption of the *p*-aminophenol group and acetate are generally examined, are simple and relatively easy to perform. However, those methods are subject to various interferences, such as bilirubin, immunoglobulin (IgM), and monoclonal immunoglobulins and their byproducts, which have similar absorption wavelengths. Moreover, these methods are susceptible with *N*-acetylcysteine (NAC) treatment, a common antidotal therapy of AP-overdose. Thus, it still remains a challenge in current clinical settings to monitor concentrations of such a small molecule accurately and rapidly for point-of-care (POC) diagnosis and decision-making in the emergency room.

In contrast to these methods, electrochemical (EC) technique is rapid, simple, and inexpensive, and has high sensitivity.[14−20] A number of modified electrodes have been fabricated and applied to the EC determination of AP levels by monitoring the redox process of ionized *p*-aminophenol in an AP sample. Although the limit of detection (LOD) could be minimized, the dynamic range and selectivity of the method remained inadequate for monitoring AP in serum samples. Because of the limited selectivity of voltammetric methods, EC approaches are mainly used as an alternative detector of spectrophotometry following chromatograhic/capillary separations. Thus, successful determination of AP in serum has not yet been demonstrated in the literature.

Here, we report for the first-time the design and fabrication of a "green" EC sensor capable of quantifying AP in serum. The sensing strategy relies on the previously unexplored strong interaction between AP and the arginine (Arg) molecule. The functional groups of AP were structurally associated with those of Arg via four hydrogen bonds, which were characterized by Fourier transform infrared spectroscopy (FTIR), ultraviolet−visible spectrophotometry (UV), and fluorescence spectroscopy. By taking advantage of this structural selectivity and high tenability of hydrogen bonds, we utilized Arg, which was immobilized on the graphene surface via electrostatic interactions, to structurally capture the AP molecule and quantify it by multiple EC sensor techniques. The optimized sensor showed similar performance in serum as in buffer, with equally good recoveries. This single-molecule recognition proof of concept, based on multihydrogen bonds (eMuHSiR) may provide a robust and highly selective approach for POC small molecule drug and biomarker detection as a promising separation-free sensory methodology.

EXPERIMENTAL SECTION

Reagents and Apparatus. Graphite flake (nature, 325 mesh) was purchased from Alfa Aesar. Arg (L-arginine), L-ascorbic acid, and phosphate buffer solution (PBS) salt were purchased from Sigma-Aldrich. AP was obtained from Fisher Scientific. All solutions were prepared with doubly distilled water. A 100 μmol/L AP stock solution was prepared with PBS buffer and kept in darkness at 4 C°.

Electrochemical measurements were performed on a CHI 660D workstation (CH instruments, USA) and Versastat 3 station (Princeton Applied Research, USA). The morphology of the samples was observed using transmission electron microscopy (TEM, Tecnai G2F30, FEI, USA). Ultraviolet visible (UV) spectra were obtained from a UV-2102 (Unico) UV−vis spectrophotometers. Fluorescence spectra were obtained from J-1500 circular dichroism (CD) Spectrometer (Jasco Inc., USA).

Synthesis of the Functionalized Graphene and Electrode Preparation. Graphene has attracted a great deal of interest due to its general electronic properties, high conductivity, good biocompatibility, and potential applications in biosensors. In this work, graphene was used as the sensor substrate. In consideration of potential clinical application, it was expected to be a nontoxic and biocompatible substrate with the potential to be produced in large quantities. Thus, graphene was synthesized through the reduction of graphite oxide (GO) using ascorbic acid, avoiding the traditional toxic reductants hydrazine or dimethylhydrazine. GO was prepared from graphite powder by using the modified Hummers method.[21] Fifty milligrams of GO was dispersed in 100 mL water to obtain a yellow-brown dispersion by ultrasonication for 12 h, and then centrifuged to remove unexfoliated GO. Subsequently, the homogeneous GO dispersion (100 mL) was mixed with 0.5 g of L-ascorbic acid, 1.0 g of L-arginine, and 0.1 of NaOH, and treated by ultrasonication for 0.5 h. The mixture was maintained at 80 °C for 12 h by heating in oil bath. After that, the mixture was cooled to room temperature, followed by another 1 h of ultrasonication. Finally, the black Arg-G was collected by filtration and further washed with water.

Experimental Procedure. All the EC experiments were carried out at room temperature using a three-electrode system in which either a modified glass carbon electrode (GC, 3 mm diameter, purchased from CHI instruments), or a gold electrode (2 mm diameter, purchased from CHI instruments), was used as the working electrode. Pt wire was used as the counter electrode and an Ag/AgCl electrode was the reference electrode.

Prior to surface modification, the bare GC was polished with 0.03 μm alumina slurry, washed successively with anhydrous alcohol and water, and natural drying at room temperature. To prepare Arg and Arg-G modified GC electrodes, Arg and Arg-G was dissolved in water with a concentration of 0.1 mg/mL. After ultrasonication for 6 h, 5 μL of Arg or Arg-G suspensions was deposited on the freshly prepared GC surface. The electrodes were dried at room temperature and were denoted as Arg/GC and Arg-G/GC, respectively.

Electrochemical cyclic voltammetry (CV) method was performed in the range from 0 to 0.60 V. The differential pulse voltammetry (DPV) parameter was as follows: increment potential, 0.004 V; pulse amplitude, 0.05 V; pulse width, 0.05 s; sample width, 0.0167 s; pulse period, 0.2 s; quiet time, 2 s. Quartz crystal microbalance (QCM) was performed on a 10 Hz electrode.

RESULTS AND DISCUSSION

Arg−AP Specific Interaction. Compared to common amino acids, the unique guanidine−NH_2 structure of Arg can strongly interact with graphene and GO.[22] In our investigation of the interactions between Arg and AP we found that,

DOI: 10.1021/acs.analchem.7b05361
Anal. Chem. 2018, 90, 4733−4740

surprisingly, as many as four hydrogen bonds can be formed between one Arg molecule and one AP molecule. Figures 1 and

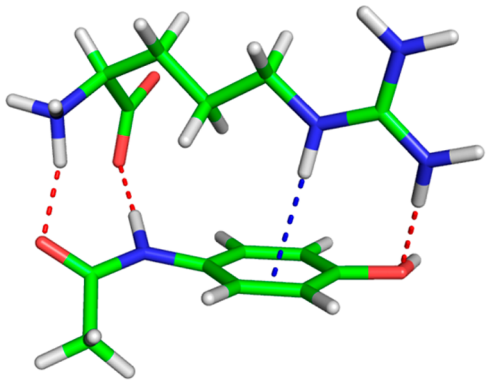

Figure 1. Optimized structure of most stable Arg−AP complex. Here, it is seen that three hydrogen bonds and one N−H···π interaction stabilize the complex.

S1 shows the potential energy minimum structure of the Arg-AP complex, as determined computationally, at the BLYP-D3/def2-TZVP level of theory. Here it can clearly be seen that the complex is stabilized by three hydrogen bonds and one N−H···π interaction.

FTIR spectroscopy was used to confirm this interaction between AP and Arg. Figure 2 shows the typical FTIR area

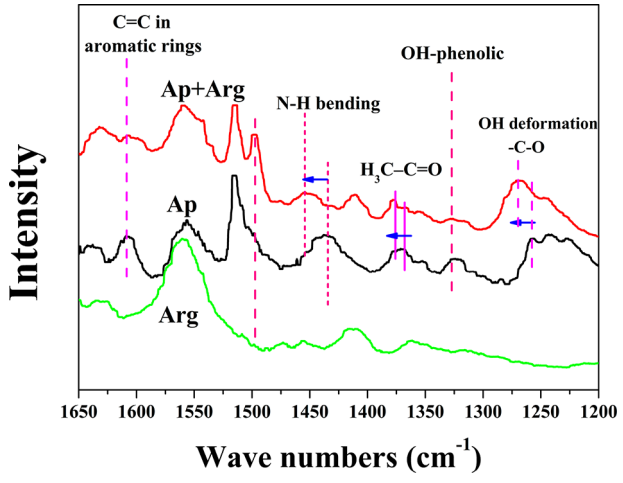

Figure 2. FTIR plots of AP, Arg, and AP + Arg composites solution.

from 1300 to 1700 cm^{-1} of AP, Arg, and AP + Arg (1:1 molar ratio) composite solution.[23] The full spectrum is displayed as Figure S2. The major bands identified in the spectrum of AP are the carbonyl vibration at 1641 cm^{-1}, the aromatic ring vibration at 1514 cm^{-1} and the OH deformation C−O stretch at 1243.5 cm^{-1}. Other bands included the H_3C−C═O stretching (1373.7 cm^{-1}), NH bending (1440.6 cm^{-1}), OH−phenolic deformation (1327 cm^{-1}), and C−NH vibration (1552.2 cm^{-1}).[24,25] While in the AP + Arg spectrum, the peak of OH deformation−C−O stretch at 1243.5 cm^{-1} in AP takes a blue shift to 1270.38 cm^{-1}, the peak at 1327 cm^{-1} assigned to the OH−phenolic deformation of AP almost disappeared in the spectrum of AP + Arg. This result indicates the formation of the hydrogen bond O···H−N, which involves a phenolic hydroxyl oxygen atom of AP and a guanidino hydrogen atom of Arg. In addition, the N−H bond peak observed at 1440.6 cm^{-1} in the AP spectrum becomes weaker and shifts to 1460.8 cm^{-1} in the spectrum of AP + Arg, indicating the formation of N−H···O interaction hydrogen bond linked an amino hydrogen atom of AP and a carboxyl oxygen atom of Arg. The π···H−N hydrogen bond between the aromatic ring of AP and −HN of Arg is implicated in the shift of C═C stretch band in aromatic rings of AP at 1607 cm^{-1} to a lower frequency after the addition of Arg. In fact, N−H···π hydrogen bonds occur frequently in biological systems, especially between the amino acid side groups in proteins and peptides.[26] Furthermore, the H_3C−C═O stretching peak appeared at 1380.7 cm^{-1} in AP + Arg rather than 1373.7 cm^{-1} of AP, which could be due to the O···H−N hydrogen bond between the acetyl oxygen atom in AP and an amino hydrogen atom of Arg. These FTIR results show four hydrogen bonds, three hydrogen bonds and an N−H···π interaction, are formed in the AP-Arg complex.

As reported previously, both AP and Arg have naturally high absorbance in the UV region. UV and fluorescence spectra have been employed to study the mechanism of action and chemical environment of AP.[27−29] Figure S3 shows the fluorescence spectra of AP, Arg, and AP + Arg in 0.1 mol/L PBS solution at pH = 7.0. AP shows a 300 nm excitation peak, and so does Arg, but the fluorescence spectra of the mixture of AP and Arg show an additional peak at 384 nm along with the other one at 293 nm. This observation is taken as further evidence of the formation of a strong complex between AP and Arg. The photodynamics of guanine could be significantly altered by the restraining conditions of the hydrogen bond interactions, which does not allow the necessary out-of-plane motions of the NH_2 group of guanine to reach the conical intersection with the ground state.[30]

To further investigate the interaction between Arg and AP, a series of experiments were performed. Figure S4 gives the UV spectra of Arg + AP at several different concentrations. It shows two high absorption peaks at 198 and 247 nm, corresponding to the n−π* transitions of the OH-phenolic group (198 nm) and the n−π* transitions of the benzene amides group (247 nm), respectively. The absorbance at 247 nm is linearly dependent on AP concentration in the range from 0.1 to 100 μmol/L, with the regression equation of A = 0.01 C (μmol/L) + 0.01 (R^2 = 0.99993), and the absorbance increases slightly after mixture with Arg. The absorbance at 198 nm, corresponding to the n−π* transitions of the OH-phenolic group in AP does not change linearly (as shown in Figure S5). The NH_2- structure of Arg could interact with the OH−phenolic group of AP to form N−H···O hydrogen bonds, which might reduce the absorbance of OH−phenolic group at 198 nm. When the [Arg]:[AP] ratio reaches 1:1, the maximum number of hydrogen bonds are formed, and the absorbance of the OH−phenolic group is the lowest one. For other ratios, the OH−phenolic group has a higher absorbance because of the decrease of hydrogen bonds.

Fabrication and Characterization of Arg−G Sensing Layer. Amino acids show a natural affinity for graphene surfaces. Interestingly, they bond to graphene surface according to the structure of their side-chain groups, and graphene-amino acid composites can be prepared by coreduction of amino acids with aqueous solutions of GO. Figure S6 shows TEM image of transparent sheets and wrinkled flake-like shapes of Arg−G indicating that it remains the perfect structure. The wrinkled surface has contributions to the high surface area of Arg−G on the electrode. One key point of our design is the Arg-bonded

DOI: 10.1021/acs.analchem.7b05361
Anal. Chem. 2018, 90, 4733−4740

graphene surface without changing the structures of Arg and graphene.

Electrochemical Behaviors of AP on the eMuHSiR Surface.

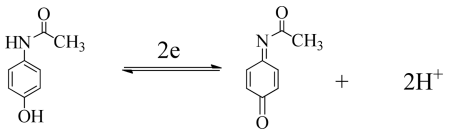

AP NAPQI (1)

The typical electrochemical reaction of AP actually is a conversion between AP and *N*-acetyl-*p*-benzoquinone imine (NAPQI), which is a toxic byproduct produced during the xenobiotic metabolism of AP, through a two-electron and two-proton process.[31] This redox process is considered as an irreversible reaction due to the instability of NAPQI in aqueous solution. It is involved decomposition, hydrolysis or hydroxylation reaction.[32−34] Thus, in Figure 3 which shows the EC

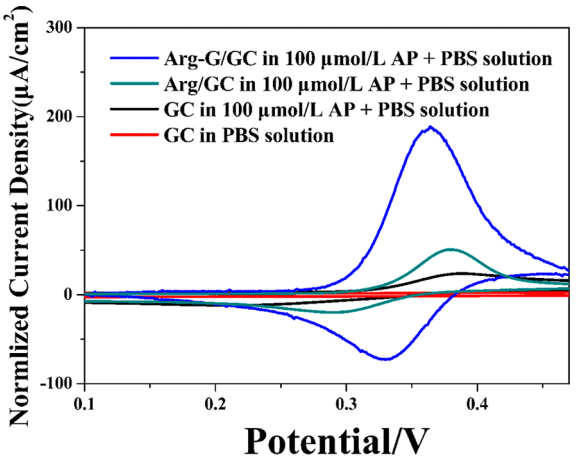

Figure 3. Cyclic voltammograms of GC, Arg/GC, and Arg-G/GC electrodes in PBS solution and/or 100 μmol/LAP + PBS solution with scan rate of 50 mV/s.

activities of AP redox reaction on the GC, Arg/GC, and Arg−G/GC electrodes in PBS aqueous solution, the anodic peak current densities are much higher than cathodic peak current densities. For GC in PBS solution without AP, no obvious peak was observed in the adopted potential range, indicating that GC is nonelectroactive in the selected potential region. In the presence of AP, the GC electrode shows a pair of AP redox peaks with relatively low current at E_{pa} = 0.388 V and E_{pc} = 0.211 V. From the green line in Figure 3, the anodic current density on Arg/GC electrode in 100 μmol/L AP solution is about 2.3 times as much as that on the bare GC, and a clear cathodic current is observed. This increased current density and improved reversibility of AP redox indicate that the electrochemical response was enhanced by capturing AP with Arg through hydrogen bonds,[35,36] even on the bare GC surface. In the case of Arg−G/GC, a pair of well-defined redox peaks of AP are observed at E_{pa} = 0.358 V and E_{pc} = 0.326 V. Obviously, the potential difference between the anodic and cathodic peaks of Arg-G/GC (32 mV) is smaller than that of GC (177 mV), which indicates that the electron transfer rate of AP redox reaction on Arg−G/GC is much faster and more reversible than that on GC. Considering the significant charge current caused by usage of graphene, the current density of Arg−G/GC in AP solution in Figure 3 is normalized by subtracting the charge current density to clearly study the Faradaic current from AP redox. As shown in Figure 3, the oxidation current density of Arg−G/GC in AP solution is about 3.5 times as much as that on the Arg/GC electrode and 8 times on bare GC electrode due to better Arg utilization and the large surface area of graphene. In our one-step Arg-G preparation, GO was reduced to graphene copresenting with Arg. Thus, Arg was able to rapidly attach on the freshly reduced graphene to in situ form Arg-G, avoiding possible structure defects caused by oxidation and surface contamination from other functional groups. This method ensures a strong electrostatic attraction between graphene and Arg, and also high Arg loading and uniform distribution of Arg on graphene, resulting in greatly improved utilization of Arg. Thus, utilization of graphene not only increased the electrode area but also facilitated the Arg utilization, as result, reflecting the high AP electrochemistry response.

The effect of scan rates was investigated on the Arg-G/GC electrode. The CVs for Arg−G/GC in 100 μmol/L AP + PBS solution with scan rates ranging from 10 to 500 mV/s are shown in Figure 4a. Both the anodic and cathodic peak currents are linearly related with the scan rates (Figure 4b) with the linear regression equation as I_{pa} (μA/cm^2) = 80.117 (μA/cm^2) + 2.847 (mA·s/Vcm^2) × v (mV/s, R^2 = 0.9976) and I_{pc} (μA/cm^2) = −36.791 μA/cm^2 − 1.767(mA·s/Vcm^2) × v (mV/s, R^2 = 0.9994), respectively. It indicates a predominantly surface-controlled process. Also of note is the peak potential shift in the scan rates from 100 to 500 mV/s (Figure S7), exhibiting a liner regression of E_p versus the logarithm of the scan rates E_{pa} = 0.4095(V) + 0.044(s) × log$v$ (V s^{-1}, R^2 = 0.989) and E_{pc} = 0.281(V) − 0.048 (s) × log v (V s^{-1}, R^2 = 0.965), respectively. According to the Laviron equation,[37,38]

$$\text{slope}_{pa} = 2.303RT/(1-\alpha)nF \quad (2)$$

$$\text{slope}_{pc} = -2.303RT/\alpha nF \quad (3)$$

the value of the electron-transfer coefficient (α) and the electron-transfer number (n) were calculated as 0.48 and 2.6, respectively. This result indicates that the reaction taking place on Arg-G/GC is a two-electron process. With eMuHSiR, the remaining adsorbed AP further enhances the electrochemical activity, which may benefit from the closer interaction of the multiple hydrogen bonds. As reported in previous publications, the mechanism of AP electrochemical oxidation is a diffusion-controlled process involving the electrochemical step and multiple chemical steps. The first step is a two-electron electrochemical oxidation to NAPQI. And the final product is p-benzoquinone after several chemical steps.[32,34,39] In Figure 4a and 4b, the peak current is direct-proportional to the scan rate, indicating a predominantly surface-controlled process rather than a diffusion-controlled one here due to AP adsorption. Unlike the covalent bond or other adsorption bonds, the strength of the hydrogen bonds is insufficient to change the chemical structure of AP. Thus, the redox reaction of AP taking place on Arg-G/GC is still a two-electron process, according to results shown in Figure 4c and 4d.

To further clarify the proton-involved redox processes eq 1 in the eMuHSiR design, the influence of solution pH on the redox reaction was studied in the range from pH 5.0 to 9.0. As shown in Figure 4c, the redox peak potentials of AP are inversely shifted with increase of pH value. A good linear

DOI: 10.1021/acs.analchem.7b05361
Anal. Chem. 2018, 90, 4733−4740

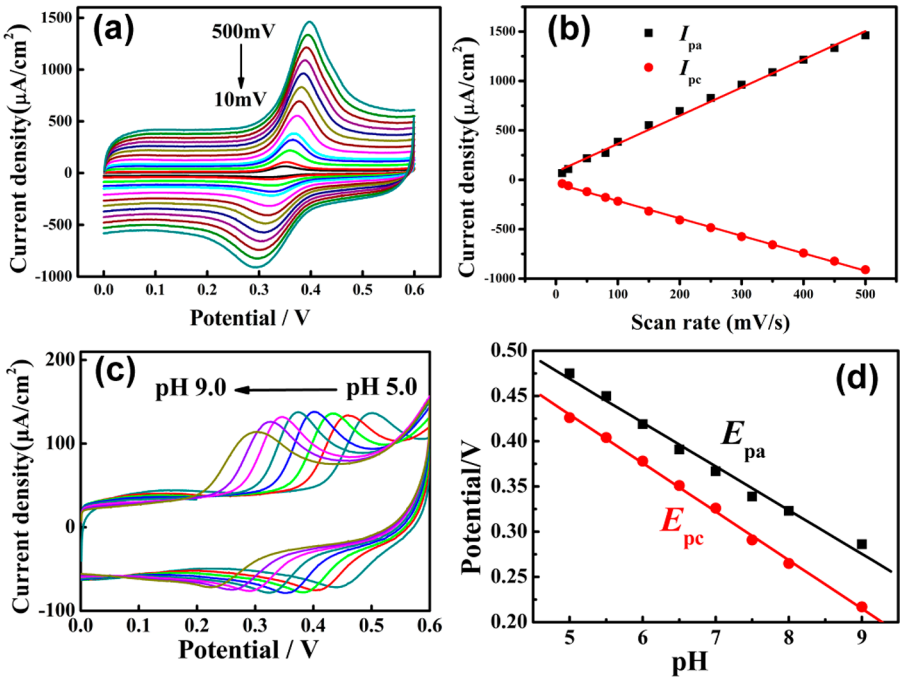

Figure 4. (a) CVs of Arg−G/GC at different scan rates (10, 20, 50, 80, 100, 150, 200, 250, 300, 350, 400, 450, and 500 mV/s) in 100 μmol/L AP+ 0.1 mol/L PBS (pH 7.0). (b) The plot of the redox peak current versus scan rate. (c) CVs of Arg−G/GC in 100 μmol/L AP under different pH values 9.0, 8.0, 7.5, 7.0, 6.5, 6.0, 5.5, 5.0. (d) The plot of anodic peak (black line) potentials and reduction peak potentials (red line) of AP versus pH values.

relationship can be established between E_p and the solution pH (Figure 4d). The regression equation can be expressed as

$$E_{pa}(V) = -0.0576(V) \times pH + 0.774(V) \quad (R^2 = 0.9979,\ \text{anodic process}) \tag{4}$$

$$E_{pc}(V) = -0.0585(V) \times pH + 0.786(V) \quad (R^2 = 0.9968,\ \text{cathodic process}) \tag{5}$$

According to the Nernst equation:[38] $dEp/dpH = 2.303mRT/nF$, where m and n are the number of protons and electrons, respectively. The slopes of above regression equations are both close to the theoretical value of 58.5 mV pH^{-1}, further indicating that the electrochemical redox of adsorbed AP remains a two-electron and two-proton process, as shown in eq 1. This is consistent with recent AP redox studies. It notes that since the DPV curve shapes and peak currents are very similar to each other in the pH range from 5−9, this reaction can be used to determine AP concentration in this wide pH range. In Figure 4c, it is clearly seen that the maximum current response is obtained around pH 7.0. Thus, this redox process is very suitable for biodetection under physiological pH. For the practical application, especially for the pharmaceutical and clinical sample, the neutral system is mostly concerned. For example, the pH range of human saliva and blood is from 6.5−7.5. In this narrow pH range, the pH effect to the hydrogen bonding is neglected.[40,41]

Sensor Technique Comparison for eMuHSiR AP Detection Design. To practically quantify AP concentrations in pharmaceutical applications and potentially human biological samples, the technique utilized for measurement should be very selective toward AP from a complex background with high sensitivity in a wide linear range covering real-life concentration levels in the sample. Since voltammetry techniques, such as CV and DPV, are low cost and rapidly responsive, they are widely used for AP study and detection.[34,42,43] Here the eMuHSiR is designed to ensure high selectivity. DPV has been performed, under optimal conditions, to investigate the relationship between the peak current and concentration of AP because of its higher sensitivity, relative to CV. Figure 5 shows DPVs

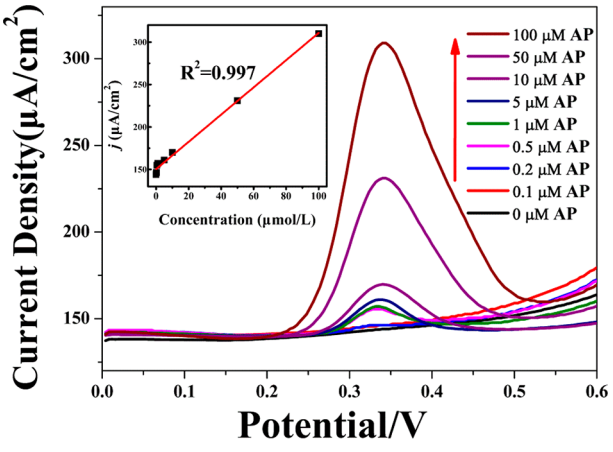

Figure 5. DPVs of 0, 0.1, 0.2, 0.5, 1, 5, 10, 50, and 100 μmol/L AP on Arg-G/GC in 0.1 mol L^{-1} PBS (pH 7.0). Inset: the plot of peak current versus AP concentration.

Arg-G/GC in 0.1 mol/L PBS (pH = 7.0) solution with different AP concentrations. The peak current density is very sensitive to the concentration change of AP. Furthermore, as can be seen in Figure 5, the oxidation peak current was proportional to AP concentration in the range from 0.5 to 100 μmol/L with the regression equation of

DOI: 10.1021/acs.analchem.7b05361
Anal. Chem. 2018, 90, 4733−4740

$$I_{pa}(\mu A/cm^2) = 1.604(\mu A/cm^2 \cdot \mu mol/L) \times C(\mu mol/L) + 148.122(\mu A/cm^2)\ (R^2 = 0.997) \quad (6)$$

The DPV of bare Au electrode in Figure S8 and eq S1 also shows Arg−G/GC has a much better sensitivity for AP than pure Au electrode. The detection limit was 0.05 μmol/L (S/N = 3), which is much lower than those obtained on GC modified with nano-TiO_2/polymer (2.0 μmol/L),[44] Nafion/TiO_2-graphene (0.21 μmol/L).[45] The good performance of the eMuHSiR sensor can be attributed to the high adsorption capacity and conductivity of positively charged Arg-G.

Several analytical techniques, such as UV, voltammetry, electrochemical impedance spectroscopy (EIS), QCM, and many other methods have been proposed for small molecule detection. UV is mostly used for the qualitative or quantitative determination of different analytes, such as transition metal ions, highly conjugated organic compounds, and biological macromolecules. As mentioned above, AP has strong absorptions in the UV range. Thus, it could be used to measure the purified AP sample with a wide linear range and relatively high sensitivity as listed in Table 1.

Table 1. Linear Range, Sensitivity, and Detection Limit for UV, CV, EIS, QCM, and DPV

method	linear range (μmol/L)	sensitivity	detection limit (mol/L)
UV	0.1−100	0.01 A/(μmol/L)	1.0×10^{-7}
EIS	12.5−100	4.73 Ω/(μmol/L)	1.0×10^{-6}
QCM	50.5−1000	3.557 Hz/(μmol/L)	2.67×10^{-6}
CV	5−100	1.01 μA·cm^{-2}/(μmol/L)	1.0×10^{-7}
DPV	**0.5−100**	**1.60 μA·cm^{-2}/(μmol/L)**	**5.0×10^{-8}**

EIS could be applied not only to simple heterogeneous electrotransfer reactions of solution components but also to more complicated electrochemical systems, such as those with coupled homogeneous reactions with absorbed intermediates. Utilizing the EIS method, the concentration of AP on the eMuHSiR surface could be quantified by measuring the surface conductivity, since the AP adsorption may reduce the AC charge transfer across the surface. Similar to other EIS sensors, the concentration of AP is expressed in the linear relationship with the real part of the Z intercept value of Nyquist plot in the 12.5−100 μmol/L range, as summarized in Table 1. However, this technique is significantly affected by electrode surface roughness and heterogeneity. Consequently, the signals are not stable enough to meet the measurement needs in practical applications and sensitivity toward small molecule adsorption is typically low.

QCM has been used in many types of electrochemical studies involving adsorption process, including the under-potential deposition of metals, adsorption/desorption of surfactants, and changes in polymer films during redox processes. However, QCM usually is highly sensitive to analytes with high molecular weight. Additionally, the selectivity of QCM is solely dependent on the surface design, making it prone to interferences by other compounds, especially when their molecular weights are similar or higher than analyte. As a small molecule, the mass change caused by AP adsorption is relatively small, hence a relatively low sensitivity (Figure S9).

In Table 1, DPV has the widest linear range, the lowest detection limit and high sensitivity, making it the most suitable technique for eMuHSiR to detect AP among the listed five methods. In addition, to estimate the fabrication reproducibility of Arg−G/GC, the proposed electrochemical sensor was evaluated by repeating the determination of 100 μmol/L AP solution. The relative standard deviation (RSD) for ten measurements was 3.75 ppt, which suggests acceptable repeatability and precision of eMuHSiR. The stability of the Arg−G/GC electrode was evaluated by repeating DPV measurements in 100 μM AP + PBS solution for 11 h, as shown in Figure S10. The anodic peak current still remained at 99.6% of the first test after 11 h. Even after 30 days, the current drop of the Arg−GC/GR system was lower than 3%. After storage at 4 °C for 2 months, it still exhibited <5% of variability from the initial response, indicating good long-term stability of the eMuHSiR surface.

Determination of AP in Pharmaceutical Tablet and Mouse Serum Samples with eMuHSiR Sensor. As a benefit of the high sensitivity and LOD of this method, we could measure the diluted sample in the PBS buffer solution, in which the pH variation was lower than 0.02 between the different samples. Additionally, it also maintains a relative constant ionic strength of solution to avoid the possible ionic strength effect to the hydrogen bonds. To test the practical application of the proposed method, the eMuHSiR was applied to analyze an AP (500 mg/tablet) tablet in comparison with the classic UV−vis and HPLC approach. All the samples were determined in quintuplicate under the same conditions, and the results are shown in Table 2. No significant difference in the testing results

Table 2. Determination of AP in Commercial Tablets (Declared as 500 mg/tablet) with UV, HPLC, and eMuHSiR

method	measured value (mg/tablet) (at 95% confidence level)
HPLC	524.4 ± 18.4
UV−vis	497.5 ± 35.8
eMuHSiR	505.4 ± 25.6

of commercial tablet at 95% confidence level was seen among the three methods. The content of AP in the tablet was calculated to be 500 mg per tablet on average, which is in good agreement with the label amount.

Detection of AP in biological samples is generally affected by uric acid (UA) and dopamine (DA).[45] Thus, experiments with interferences of UA and DA on AP detection of Arg−G/GC were conducted. Figure S11 shows CVs of the Arg−G/GC in 0.1 M BPS (pH 7.0) solution containing 0.1 mmol/L UA, 0.1 mmol/L DA and 0.1 mmol/L AP at scan rate of 50 mV/s. AP exhibits a well-defined wave with good separations from UA and DA on Arg−G/GC, Therefore, excellent selectivity of AP on Arg−G/GC is achieved. In addition, other influences from common coexisting substances were also investigated. The presence of inorganic species K^+, Na^+, NH_4^+, Ca^{2+}, Mn^{2+}, Cd^{2+}, Zn^{2+}, Cu^{2+}, Al^{3+}, Cl^-, Ac^-, SO_4^{2-}, and PO_4^{3-} at a 100-fold higher concentration and *p*-aminophenol, glucose, vitamin C, caffeine, xanthine, *N*-acetylcysteine, and tyrosine at 50-fold higher concentration has no significant effect on the detection of 100 μmol/L AP when the peak current change is below 5%. In this work, AP redox reaction on the GC, Arg/GC, and Arg−G/GC electrodes occurred at the typical AP redox potential. Apart from the anodic potential of AP as described in previous work,[46−50] the structured multihydrogen bonds adsorption produces the additional selectivity for the AP redox reaction. The Arg receptor can adsorb AP from solution and increase the

DOI: 10.1021/acs.analchem.7b05361
Anal. Chem. 2018, 90, 4733−4740

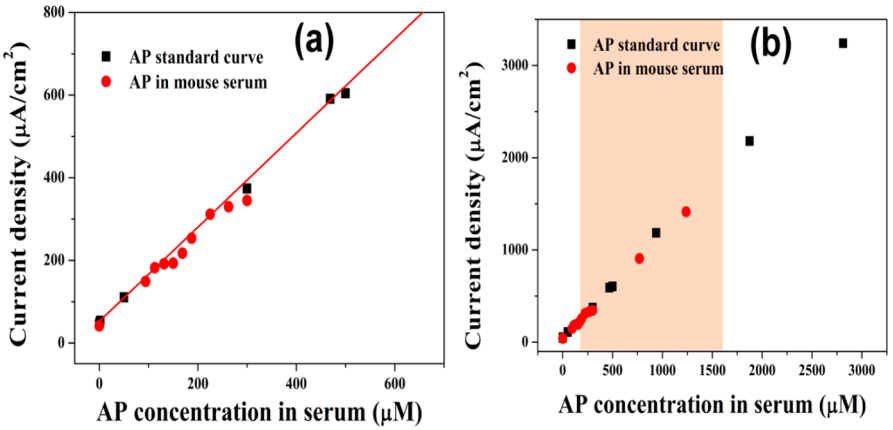

Figure 6. Relationship of peak current in serum with low AP concentration (a) and high AP concentration (b).

number of AP molecules on the electrode taking redox reactions. Thus, this technique can be applied on the complex serum samples measurement.

Clinically, AP poisoning can cause gastroenteritis within hours and hepatotoxicity 1 to 3 days after ingestion. Severity of hepatotoxicity after a single acute overdose is predicted by AP levels in serum. For a single acute overdose of traditional AP or rapid-relief AP (which is absorbed 7 to 8 min faster), levels are measured ≥4 h after ingestion and plotted on the nomogram. A level ≥1300 μmol/L after 4 h ingestion, or a level ≥300 μmol/L after 8 h ingestion indicate possible hepatotoxicity.[51] Thus, it is significant to detect AP in serum in a wide concentration range from 200 to 1600 μmol/L (shaded area in Figure 6b). An AP standard curve in PBS buffer solution (sample 1) was established using the eMuHSiR sensor and used to quantify AP in mouse serum (sample 2). When serum sample and PBS were mixed at less than 1:1 volume ratio, measured data show a wide linear range in high fidelity to values in PBS buffer (Figure 6a). The substances in serum, such as sugars and lipids, have almost no interference with the detection of AP. When the blood sample and buffer solution mixing ratio was more than 1:1, the serum measurement exhibited the declined peak current. It may be due to increased viscosity caused by the amount of nonelectrolyte in serum. Under optimized conditions, the eMuHSiR showed a wide linear detection range of 1−3000 μmol/L of AP (Figure 6b). Because of the selective adsorption and high electrochemical response, the interferences from other species in the blood are neglected in this test. These results demonstrate a great potential for the eMuHSiR detection method of AP to be tested in the clinic.

Compared to current AP detection designs shown in Table S1, eMuHSiR provides a label-free, green, low-cost, and biocompatible AP sensor. And it has the potential to adjust sensor performance by changing AP loading and electrode area. The linear range, sensitivity and LOD of current design are tailored to meet both pharmaceutical and clinical settings. Specifically, Arg−G mediated AP selective adsorption results in greatly enhanced sensor selectivity, improving upon limitations of current detection methods and facilitating utility in complex and high throughput clinical applications.

CONCLUSIONS

In this work, we discovered a new rapid and highly specific small molecule detection method developed for the AP POC analysis, in which AP molecules were allowed to structure-selectively interact with Arg molecules by forming four intermolecular hydrogen bonds. The Arg functionalized graphene was produced successfully by an environmental-friendly method, which exhibited high EC activity and selectivity for the AP quantification. The enhanced redox peak current of AP is attributable to the high adsorption capacity and conductivity of positively charged Arg−G. The extra selectivity was produced by this extreme high EC response than that would be caused by other possible active species at the same potential. Under optimized conditions, Arg−G/GC shows wide linear behavior in the range of 0.1 μmol/L to 100 μmol/L of AP with a detection limit of 0.05 μmol/L, which meets the needs for both pharmaceutical measurement and clinical blood testing. In this study the possible effect from the solution's ionic strength is still under investigation. To a certain extent, higher ionic strength could weaken hydrogen bonds. While for a specific biosystem, the local environment may play a far greater role in hydrogen bonding strengths and lengths. Since this highly selective EC method was fundamentally built on molecular-level functional group recognition, it overcomes the major barrier of biosensors for practical applications. We conclude that this method offers superior sensitivity and selectivity without the need for any extra separation process. For the future clinical testing, we plan to use the disposable strip electrode to conduct human blood measurement. More results will be reported in the future publication.

Briefly looking to the future, a reasonable extrapolation of our current data leads us to expect that by designing specific interface acceptor structures and customizing electrode materials, it may be possible to do the following: (1) achieve both sensitivity and selectivity for the detection of a wide variety of small molecules using an electrode element; (2) reduce the time scale for real-time detection and the study of molecular binding kinetics; and (3) implement parallel-array assays for high-throughput point-of-care applications while maintaining extremely low sample volume requirements. Finally, the instrumental simplicity of the EC approach is expected to greatly facilitate field-portable conditional or point-of-care medical diagnostic applications.

ASSOCIATED CONTENT

Supporting Information

The Supporting Information is available free of charge on the ACS Publications website at DOI: 10.1021/acs.analchem.7b05361.

DOI: 10.1021/acs.analchem.7b05361
Anal. Chem. 2018, 90, 4733−4740

(PDF)

AUTHOR INFORMATION

ORCID

Guangdi Wang: 0000-0002-3999-8213
Zhe Wang: 0000-0003-3762-3167

Author Contributions

Y.Z. and Z.H. are equally contributed to this work.

Notes

The authors declare no competing financial interest.

ACKNOWLEDGMENTS

This publication was made possible by funding from the NIMHD-RCMI (5G12MD007595), the NIGMS-BUILD (8UL1GM118967), NIH-RTRN (U54MD008149), and National Science Foundation (Grant HRD-1700429). This publication was also made possible by the Louisiana Cancer Research Consortium. The contents are solely the responsibility of the authors and do not necessarily represent the official views of the NIMHD. K.R. gratefully acknowledges support from the NSF HBCU-UP program (HRD-1505219) and the NIH R15 program (1R15GM113193-01). Dr. Zhe Wang also thanks Dr. Dan He and Ms. Patricia Pham's supporting work.

REFERENCES

(1) Nourjah, P.; Ahmad, S. R.; Karwoski, C.; Willy, M. *Pharmacoepidemiol. Drug Saf.* **2006**, *15*, 398−405.
(2) Holubek, W. J.; Kalman, S.; Hoffman, R. S. *Hepatology* **2006**, *43*, 880−880.
(3) Ryder, S.; Beckingham, I. *Brit Med. J.* **2001**, *322*, 290.
(4) Bruns, C. A. B. D. E. *Tietz Fundamentals of Clinical Chemistry and Molecular Diagnostics*; Elsevier Health Sciences, 2014.
(5) Hung, O. L.; Nelson, L. *Tintinalli's Emergency Medicine: A Comprehensive Study Guide*; McGraw-Hill: New York, 2004.
(6) Bizovi, K. E.; Aks, S. E.; Paloucek, F.; Gross, R.; Keys, N.; Rivas, J. *Ann. Emerg Med.* **1996**, *28*, 549−551.
(7) Cetarukcol, E. W.; Dartcol, R. C.; Hurlbutcol, K. M.; Horowitzcol, R. S.; Shihcol, R. *Ann. Emerg Med.* **1997**, *30*, 104−108.
(8) Burtis, C. A.; Bruns, D. E. *Tietz Fundamentals of Clinical Chemistry and Molecular Diagnostics*; Elsevier Health Sciences, 2014.
(9) Heard, K. J. *N. Engl. J. Med.* **2008**, *359*, 285−292.
(10) Alkharfy, K. M.; Frye, R. F. *J. Chromatogr., Biomed. Appl.* **2001**, *753*, 303−308.
(11) Burgot, G.; Auffret, F.; Burgot, J.-L. *Anal. Chim. Acta* **1997**, *343*, 125−128.
(12) Perez-Ruiz, T.; Martinez-Lozano, C.; Tomas, V.; Galera, R. *J. Pharm. Biomed. Anal.* **2005**, *38*, 87−93.
(13) Ruengsitagoon, W.; Liawruangrath, S.; Townshend, A. *Talanta* **2006**, *69*, 976−983.
(14) Kang, X.; Wang, J.; Wu, H.; Liu, J.; Aksay, I. A.; Lin, Y. *Talanta* **2010**, *81*, 754−759.
(15) Yu, D.; Renedo, O. D.; Blankert, B.; Sima, V.; Sandulescu, R.; Arcos, J.; Kauffmann, J.-M. *Electroanalysis* **2006**, *18*, 1637−1642.
(16) Goyal, R. N.; Gupta, V. K.; Oyama, M.; Bachheti, N. *Electrochem. Commun.* **2005**, *7*, 803−807.
(17) Sun, D.; Zhang, H. *Microchim. Acta* **2007**, *158*, 131−136.
(18) Song, J.; Yang, J.; Zeng, J.; Tan, J.; Zhang, L. *Sens. Actuators, B* **2011**, *155*, 220−225.
(19) Quintino, M. S. M.; Araki, K.; Toma, H. E.; Angnes, L. *Electroanalysis* **2002**, *14*, 1629−1634.
(20) Kumar, S. A.; Tang, C.-F.; Chen, S.-M. *Talanta* **2008**, *76*, 997−1005.
(21) Hummers, W. S.; Offeman, R. E. *J. Am. Chem. Soc.* **1958**, *80*, 1339−1339.
(22) Guo, Y.-n.; Lu, X.; Weng, J.; Leng, Y. *J. Phys. Chem. C* **2013**, *117*, 5708−5717.
(23) Ramos, M. L.; Tyson, J. F.; Curran, D. J. *Anal. Chim. Acta* **1998**, *364*, 107−116.
(24) Ebrahimi, A.; Saffari, M.; Dehghani, F.; Langrish, T. *Int. J. Pharm.* **2016**, *499*, 217−227.
(25) Terzyk, A. P. *Colloids Surf., A* **2001**, *177*, 23−45.
(26) Trachsel, M. A.; Ottiger, P.; Frey, H.-M.; Pfaffen, C.; Bihlmeier, A.; Klopper, W.; Leutwyler, S. *J. Phys. Chem. B* **2015**, *119*, 7778−7790.
(27) Bertolini, A.; Ferrari, A.; Ottani, A.; Guerzoni, S.; Tacchi, R.; Leone, S. *CNS Drug Rev.* **2006**, *12*, 250−275.
(28) Moyon, N. S.; Singh, T. S.; Mitra, S. *Biophys. Chem.* **2008**, *138*, 55−62.
(29) Meyer, J.; Karst, U. *Chromatographia* **2001**, *54*, 163−167.
(30) Zelený, T. s.; Ruckenbauer, M.; Aquino, A. J.; Müller, T.; Lankaš, F.; Dršata, T. s.; Hase, W. L.; Nachtigallova, D.; Lischka, H. *J. Am. Chem. Soc.* **2012**, *134*, 13662−13669.
(31) Kumar, S. A.; Tang, C.-F.; Chen, S.-M. *Talanta* **2008**, *76*, 997−1005.
(32) Shafiei, H.; Haqgu, M.; Nematollahi, D.; Gholami, M. *International Journal of Electrochemical Science* **2008**, *3*, 1092−1107.
(33) Nematollahi, D.; Shayani-Jam, H.; Alimoradi, M.; Niroomand, S. *Electrochim. Acta* **2009**, *54*, 7407−7415.
(34) Miner, D. J.; Rice, J. R.; Riggin, R. M.; Kissinger, P. T. *Anal. Chem.* **1981**, *53*, 2258−2263.
(35) Matta, C. F.; Hernández-Trujillo, J.; Tang, T.-H.; Bader, R. F. W. *Chem. - Eur. J.* **2003**, *9*, 1940−1951.
(36) Kato, T.; Frechet, J. M. J. *J. Am. Chem. Soc.* **1989**, *111*, 8533−8534.
(37) Bard, A.; Faulkner, L. *Electrochemical Methods: Fundamentals and Applications*; John Wiley & Sons, Inc., 2001.
(38) Laviron, E. *J. Electroanal. Chem. Interfacial Electrochem.* **1974**, *52*, 355−393.
(39) Valero, E.; Carrión, P.; Varón, R.; García-Carmona, F. *Anal. Biochem.* **2003**, *318*, 187−195.
(40) Wood, J. L. *Biochem. J.* **1974**, *143*, 775−777.
(41) Stockton, W.; Rubner, M. *Macromolecules* **1997**, *30*, 2717−2725.
(42) Sanghavi, B. J.; Srivastava, A. K. *Electrochim. Acta* **2010**, *55*, 8638−8648.
(43) Tavana, T.; Khalilzadeh, M. A.; Karimi-Maleh, H.; Ensafi, A. A.; Beitollahi, H.; Zareyee, D. *J. Mol. Liq.* **2012**, *168*, 69−74.
(44) Kumar, S. A.; Tang, C. F.; Chen, S. M. *Talanta* **2008**, *76*, 997−1005.
(45) Fan, Y.; Liu, J.-H.; Lu, H.-T.; Zhang, Q. *Colloids Surf., B* **2011**, *85*, 289−292.
(46) Chen, X.; Zhu, J.; Xi, Q.; Yang, W. *Sens. Actuators, B* **2012**, *161*, 648−654.
(47) Amiri-Aref, M.; Raoof, J. B.; Ojani, R. *Sens. Actuators, B* **2014**, *192*, 634−641.
(48) Menon, S.; Jesny, S.; Girish Kumar, K. *Talanta* **2018**, *179*, 668−675.
(49) Huang, T.-Y.; Kung, C.-W.; Wei, H.-Y.; Boopathi, K. M.; Chu, C.-W.; Ho, K.-C. *J. Mater. Chem. A* **2014**, *2*, 7229−7237.
(50) Manjunatha, R.; Nagaraju, D. H.; Suresh, G. S.; Melo, J. S.; D'Souza, S. F.; Venkatesha, T. V. *Electrochim. Acta* **2011**, *56*, 6619−6627.
(51) Chiew, A. L.; Fountain, J. S.; Graudins, A.; Isbister, G. K.; Reith, D.; Buckley, N. A. *Med. J. Aust.* **2015**, *203*, 215−218.

DOI: 10.1021/acs.analchem.7b05361
Anal. Chem. 2018, 90, 4733−4740